ELSEVIER

Thin Solid Films 415 (2002) 258–265

thin solid films

www.elsevier.com/locate/tsf

Surface modification of ion-implanted AISI 304 stainless steel after oxidation process: X-ray absorption spectroscopy analysis

F.J. Pérez[a,*], A. Gutierrez[b], M.F. López[c], M.P. Hierro[a], F. Pedraza[a]

[a]*Universidad Complutense de Madrid. Departamento CC Materiales, 28040 Madrid, Spain*
[b]*Universidad Autónoma de Madrid. Dpto Física Aplicada. Cantoblanco. 28049, Madrid, Spain*
[c]*Consejo Superior de Investigaciones Científicas. Instituto de Ciencia de Materiales de Madrid. Dpto. Física e Ingeniería de Superficies. Cantoblanco 28049-Madrid, Spain*

Received 29 November 2001; received in revised form 20 February 2002; accepted 11 April 2002

Abstract

The influence of implanted Si, Mo and Ce vs. the as-received austenitic AISI 304 stainless steel has been studied after isothermal oxidation in air at 900 °C for 32 h. The oxide layer formed was characterised by means of conventional X-ray diffraction, scanning electron microscopy/energy-dispersion spectroscopy and X-ray absorption spectroscopy (XAS) techniques. The projected ranges of the implantation were calculated using the TRIM code. The results obtained by the most sensitive technique, XAS, show slight differences in the chemical composition of the oxide layer of the different ion-implanted samples. However, these chemical differences could determine a threshold between acceptable and non-acceptable oxidation behaviour. The evolution of the chemical composition from the oxide–metal interface to the oxide surface has also been studied. XAS spectra show that Cu diffusion is favoured in the oxide layer for the non-implanted sample, which does not occur for implanted samples. Both Si and Ce ion implantation promotes active diffusion of Cr and Mn from the parent steel to form a protective oxide layer, whereas Mo implantation induces major participation of Fe in the oxide scale. This may have been caused because of volatilisation of molybdenum oxides.

Keywords: Ion implantation; Oxidation; X-Ray absorption; X-Ray diffraction

1. Introduction

Alloy steels with adequate high-temperature strength, such as those commonly employed in petrochemical or electric power plants, etc., have poor oxidation, sulfidation and hot corrosion resistance [1]. Steels designed to withstand these oxidising or sulfidising environments rely on the formation of Cr_2O_3 or Al_2O_3 scales [2–4]. Specifically, the finishing sections of the tubing and the pipes that take steam to the high-pressure turbine in fossil-fuel-fired boilers are typically manufactured either in Cr–Mo ferritic steels or in the austenitic AISI 304 stainless steel [5]. These stainless steels are designed to develop a protective Cr_2O_3 oxide scale upon oxidising conditions up to approximately 900 °C, at which temperature further oxidation into volatile CrO_3 species takes place [6].

One of the current trends (in research and production) is to slightly modify the surface of different metals and alloys in order to take advantage of their known manufacturing techniques. Ion implantation offers the unique possibility to introduce a controlled concentration of an element to a thin surface layer. In addition, this technique induces changes in the surface due to radiation damage [7–9] without changing the original dimensions of the part to be treated. Small amounts of the so-called reactive elements (RE) added to the outer surface of the metals, and alloys have been reported to decrease the oxidation rate and improve the scale adherence [10,11], leading to an overall beneficial effect.

The successful application of surface modification techniques also involves characterisation of the implant. To investigate the influence of ion implantation on the oxidation behaviour of AISI 304 stainless steel, it is important to evaluate the chemical composition of the oxide layer formed at high temperature. Due to the thickness of this outer layer, one of the most appropriate

*Corresponding author. Tel.: +34-91-394-4215; fax: +34-91-394-4357.
E-mail address: fjperez@eucmos.sim.ucm.es (F.J. Pérez).

0040-6090/02/$ - see front matter © 2002 Elsevier Science B.V. All rights reserved.
PII: S0040-6090(02)00359-0

Table 1
Projected ranges (Rp) of the implanted ions calculated by TRIM computer simulation

	Si-implanted	Mo-implanted	Ce-implanted
$Rp \pm \Delta Rp$ (Å)	982 ± 397	358 ± 113	308 ± 78

techniques was found to be X-ray absorption spectroscopy (XAS) due to its sampling depth. XAS is an analytical technique that measures the effect where an electron is promoted from a core-level state to an empty, excited electronic state. When XAS is used in the total electron-yield mode, all escaping electrons are recorded. In this case, the probe depth is $\approx 70-100$ Å for the transition metal 2p edges [12,13], which is larger than that of XPS and AES (≈ 20 Å). XAS is thus a powerful tool for obtaining information on the chemical composition of materials [14–16].

This work investigates the influence of ion implantation of different elements on the chemical composition of the oxide scale grown on a commercial AISI 304 stainless steel after having been isothermally oxidised at 1173 K for 32 h under atmospheric pressure of air. Mass gains and X-ray diffraction (XRD), as well as scanning electron microscopy/energy-dispersive spectroscopy (SEM/EDS), were used to characterise the bulk oxide scales, whereas XAS studies were carried out to characterise the specific features of the main oxide.

2. Experimental

Specimens of austenitic AISI 304 stainless steel (SS) measuring $15 \times 3.5 \times 1$ mm^3 with a nominal chemical composition of (wt.%): 18.2 Cr; 9.4 Ni; 1.5 Mn; 0.4 Si; 0.2 Mo; 0.2 Cu; 0.1 Co; 0.047 C; 0.027 P; 0.005 N; 0.003 S; 0.003 Ti; and 0.002 Al (balance Fe) were investigated. Before testing, the samples were mechanically polished with SiC emery paper up to #600, and then ultrasonically degreased in acetone.

Si, Mo and Ce ion implantation was carried out at an energy of 150 keV with ion doses of 1×10^{15} Si/cm^2, 1×10^{14} Mo/cm^2 and 1×10^{14} Ce/cm^2. Table 1 shows the projected ranges (Rp) and their standard deviations (ΔRp) for the different implanted ions. These Gaussian distributions were calculated by computer simulation using the TRIM code, assuming a 50-Å-thick passive layer on the stainless steel.

The implanted and non-implanted specimens were oxidised in a muffle furnace under atmospheric pressure of air for periods of up to 32 h. Conventional XRD was performed in a Philips X'Pert instrument using CuK_α radiation. The morphology of the scales was observed by SEM and analysed by EDS in a JEOL ISM 35C at 20 kV with a coupled Kevex 7077 microanalyser.

For comparative purposes and as reference materials, the following samples were also studied by XAS: (a) as-received AISI 304 stainless steel sample; (b) Fe and Cr pure metal samples, in the form of polycrystalline material (these samples were abraded in situ in the UHV chamber with a diamond file to measure the clean metal surfaces); and (c) FeO, oxidised Fe, and oxidised Cr samples. Oxidised samples of Fe and Cr were produced by exposure of the metal samples in air, spontaneously generating the specific oxide layer on each sample surface. The FeO sample consisted of a pressed pellet of FeO powder, which was also subsequently abraded in situ in the UHV chamber with a diamond file to remove surface contaminants.

The XAS measurements were carried out at a PM-1 soft X-ray monochromator at the Berliner Elektronenspeicherring für Synchrotronstrahlung (BESSY). XAS spectra were obtained at the transition metal 2p absorption thresholds (Cr, Fe, Ni, Cu and Mn), and at the Mo 3p, Ce 3d and oxygen 1s absorption thresholds by recording the total yield of secondary electrons from the sample surfaces, i.e. in TEY mode. The base pressure in the UHV chamber during the measurements was better than 2×10^{-10} mbar. In order to provide in-depth information on the oxidised states of the elements of interest, diamond abrasion of the outermost oxide layers was also performed in the UHV chamber, disregarding ion sputtering so as to avoid the likely reduction of the metallic oxides.

3. Results and discussion

The differences in the Rp values arise from the relation between the accelerating voltage, the incidence angle, the type of substrate atoms and their binding energy, and the type of incident atom [17]. Since only the latter parameter was varied, the heavier ions resulted in a lower implantation depth, which is in agreement with the results shown in Table 1.

The results of the overall mass gain per surface unit after 32 h of isothermal oxidation are shown in Fig. 1. It can be readily observed that the Ce-implanted specimens undergo the least oxidation, followed by the non-implanted steel. The Si-implanted steel showed the smallest weight increase. However, the results for Mo-implanted steel show a different trend of mass loss, indicative of oxide scale spallation. Since all the different specimens tested have undergone the same heat treatment, the extent of spallation could be indicative of a different oxide-scale morphology and/or nature on each sample. The as-received AISI 304 steel did not suffer any spalling of the oxide scale, whereas the Si- and Ce-implanted samples showed small spalled areas after cooling in air. This could be explained in terms of the relaxation of the stresses induced by the implantation process. Spallation was more significant in the Mo-implanted samples, giving rise to an overall mass loss. Such extensive spallation could be related to the for-

mation of molybdenum oxides, such as MoO_2 and MoO_3, which may become volatile at temperatures above 600 °C [18].

The oxidised species were identified by X-ray diffraction, as shown in Table 2, in which the species are presented by order of importance (by peak intensity and width). The f.c.c. austenite (γ) peak is identified in both the as-received and Mo-implanted steel as the major species. This is in contrast to the b.c.c. ferrite (α) phase identified as the most important species in the Si- and Ce-implanted specimens. This could indicate that enhanced oxidation of Cr takes place, which induced a γ (f.c.c.) $\rightarrow \alpha$ (b.c.c.) transformation by diffusion from the bulk alloy to the oxide layer. It is well known that chromium can stabilise the ferrite phase. It can also be observed that the main oxidised compound is $Cr_{1.3}Fe_{0.7}O_3$ in all species, except for the case of the Mo-implanted steel, for which an Fe-rich oxide of composition $(Fe_{0.6}Cr_{0.4})_2O_3$ is formed. This fact may imply that Mo may hinder outward cation diffusion to a certain extent, or that XRD provides information about the oxide phases grown at the original oxide scale/substrate interface before spallation, as is further discussed below. An interesting point is that all oxidised specimens have developed a spinel-like oxide enriched in Mn ($Mn_{1.5}Cr_{1.5}O_4$). The presence of these spinels has previously been observed on the same stainless steel exposed for longer oxidation times (500 h) at 900 °C [19]. Such spinels were reported to have grown at the outermost part of the oxide scale, where this type of compound gives the most protective effects.

The high-magnification SEM surface morphology of all oxidised specimens, showing differences between the compact oxide scales, is shown in Fig. 2. It can be observed that all the oxide scales have grown following the ridges and valleys marked from the surface finish (SiC#600) of the metal substrate. As is well known, ion implantation induces defects, such as voids or stressed areas on the implanted material, and thus diffusion of the alloying elements is subsequently enhanced upon high-temperature exposure. It can be observed that the scales are very compact with a very small crystal size, which may in turn impede anion and/or cation diffusion. However, the Mo-implanted steel shows cavities in the compact oxide scale. The origin of these cavities could be the formation of volatile molybdenum oxides, which may be able to break the oxide scale during vaporisation at high temperature. These cavities could act as diffusion paths through which oxidation may proceed. As a result, the Mo-implanted specimens may degrade more rapidly than the remaining samples upon further oxidation. The surface EDS microanalysis showed the same spectra, with Cr and Mn enrichment on the oxide scale grown on the as-received and all implanted specimens. This confirms the identification of the spinel-like oxides observed by means of XRD.

Table 2
XRD species identified after oxidation of the specimens in air at 900 °C for 32 h

Material	Species
As-received	γ, α, $Cr_{1.3}Fe_{0.7}O_3$, $Mn_{1.5}Cr_{1.5}O_4$
Si-implanted	α, γ, $Cr_{1.3}Fe_{0.7}O_3$, $Mn_{1.5}Cr_{1.5}O_4$
Mo-implanted	γ, α, $(Fe_{0.6}Cr_{0.4})_2O_3$, $Mn_{1.5}Cr_{1.5}O_4$
Ce-implanted	α, γ, $Cr_{1.3}Fe_{0.7}O_3$, $Mn_{1.5}Cr_{1.5}O_4$

Fig. 3 shows the Cr 2p soft X-ray absorption spectra of all AISI 304 stainless steel samples after the oxidation process, as well as oxidised Cr and non-oxidised Cr for comparison. All spectra present two broad peaks separated by the spin-orbit splitting of the Cr 2p core hole. The soft X-ray absorption spectrum of Cr_2O_3 exhibits a peak at $\approx$576.5 eV in the $2p_{3/2}$ region and a distinctive

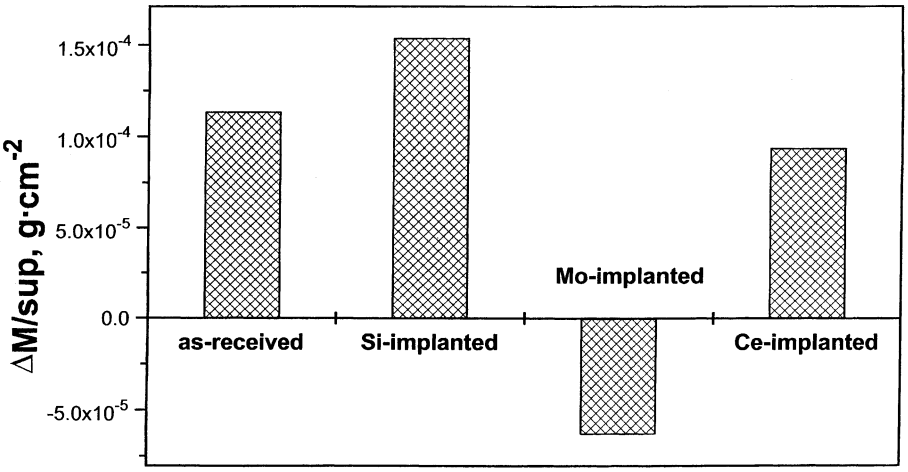

Fig. 1. Mass variations after oxidation in air at 900 °C for up to 32 h of both implanted and non-implanted materials.

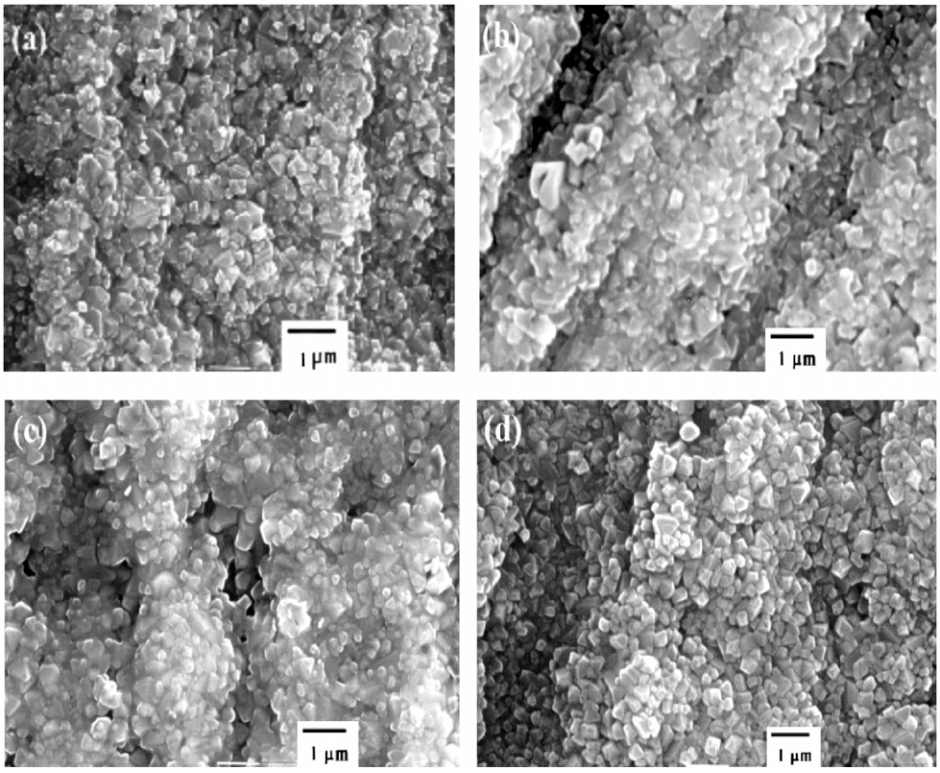

Fig. 2. SEM surface morphology of the oxide scale growth after 32 h of oxidation at 900 °C: (a) as-received material; (b) Si-implanted steel; (c) Mo-implanted steel; and (d) Ce-implanted steel.

shoulder at ≈575 eV, as can be observed in the literature. The spectrum of Cr metal has a different shape than that of Cr_2O_3, with a peak located at ≈575 eV. The oxidised Cr spectrum that corresponds to the oxide film is a mixture of metallic chromium and Cr_2O_3, since the XAS technique analyses depths of 70–100 Å. As the metallic contribution increases, so does the intensity of the shoulder at ≈575 eV. The Cr 2p spectra of all oxidised AISI 304 samples correspond to Cr_2O_3, as can be deduced by comparison with the Cr 2p spectrum of Cr_2O_3 obtained in previous work [20]. This result indicates that the presence of Cr in the oxidised layer formed on the surface of the samples is in the form of Cr. Since the probe depth of the XAS technique is smaller than the thickness of the oxidised layer (≈100 Å), no metallic Cr was expected.

Fig. 4 shows the Fe 2p soft X-ray absorption spectra for all the AISI 304 stainless steels, i.e. the as-received, and the Si-, Mo- and Ce-implanted samples, after the oxidation process. Spectra of Fe metal and FeO are also shown for comparison. All spectra consist of two broad peaks, which are separated, to a first approximation, by the spin-orbit splitting of the Fe 2p core hole. The differences observed in the background slope and the statistical data dispersion are due to the different signal/noise ratio of the different samples. The Fe 2p emission intensity is higher for the as-received and Mo-implanted samples, indicating a higher proportion of Fe compounds in the outer layers of these heat-treated steels. The intensity of the Si- and Ce-implanted samples is much lower, producing a lower signal/noise ratio and making any analysis of the L_{III} signal difficult. Concerning the L_{II} signal, the Fe 2p spectral shape is quite similar for all samples and corresponds to Fe_2O_3, as can be deduced by comparison with the Fe_2O_3 spectra of a previous study [20]. Again, the presence of metallic Fe in the oxidised layer is not observed, as can be deduced by comparing with the Fe metal spectrum.

The absorption spectra of all the AISI 304 stainless steel main constituents (Fe, Cr, Ni and Mn), as well as of the implanted elements, were measured. However, for reasons of space, only the most relevant, i.e. Cr 2p and Fe 2p, are shown. From the analysis of the XAS spectra, not only the chemical state can be obtained, but also the composition percentage of the outer layer. Fig. 5 represents the percentage composition corresponding to such main constituents at the external surface of the AISI 304 stainless steel samples, calculated from the XAS spectra. In order to obtain information on the percentage composition of the central and innermost zones of the oxidised layer, the samples were abraded with a diamond file until approximately 50 ± 10 and $80 \pm 10\%$ of the original oxide layer had been removed. Therefore, the *surface*, *middle* and near *interface* data

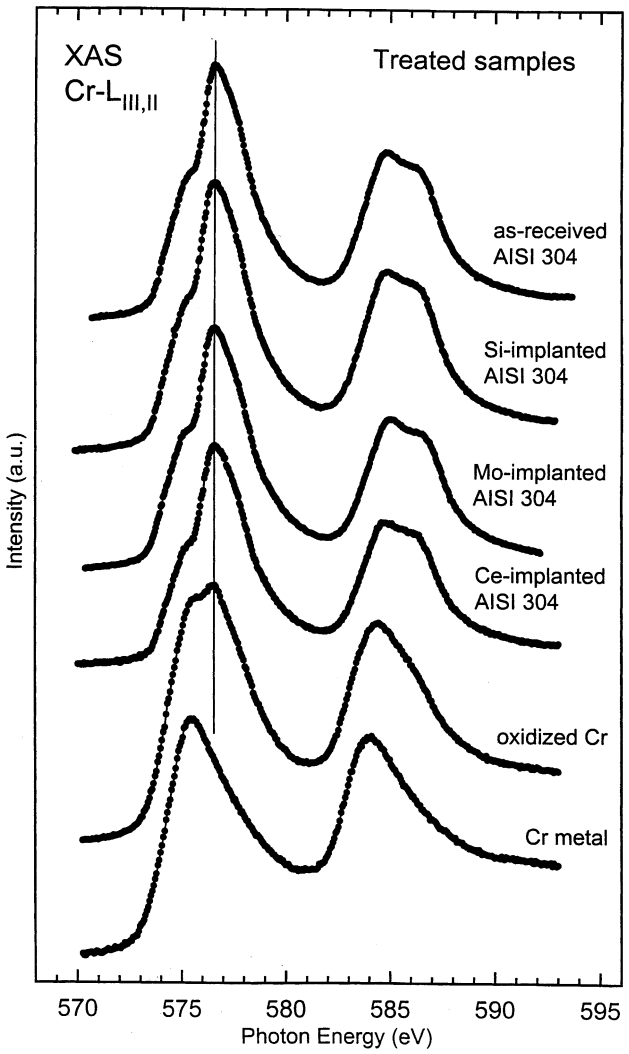

Fig. 3. Cr 2p soft X-ray absorption spectra of all heat-treated AISI 304 stainless steel samples: as-received and after Si, Mo and Ce ion implantation, and oxidised Cr and Cr metal samples for comparison.

represent the results obtained for non-abraded samples, approximately half of the oxidised layer abraded and abraded to reach the oxide–metal interface, respectively. For all samples, Fig. 5 shows a surface with Cr and Mn as main constituents of the oxidised layer. This result suggests that, during the thermal treatment, Cr and Mn are the elements most prone to react with oxygen to form the oxide phases at the external surface. Conventional XRD showed the presence of $Mn_{1.5}Cr_{1.5}O_4$ spinel oxides, whereas EDS analyses also demonstrated Cr and Mn enrichment at the oxide scale surface. Thus, the XAS results are in agreement with the findings obtained by conventional XRD, as well as with the EDS microanalysis. However, Fig. 5 exhibits a poor Fe signal for all samples, increasing with depth to become the largest component in the interface region. Therefore, an important conclusion obtained from Fig. 5 is that, although Fe is the main component of AISI 304, its diffusion is superseded by that of Cr or Mn. In fact, this figure also shows that the oxide layer mostly consists of MnO and Cr_2O_3 at the surface (or a solid solution of these), and decreasing depth of the oxide shows decreasing amounts of iron and nickel oxides. This can be explained by the variation in phase composition with increasing depth, with the subsequent decrease in oxygen potential [21]. In fact, in the oxide layer all cationic species diffuse according to the chemical potential at that level.

It can be also observed that the Mo-implanted sample has the largest amount of Fe and Ni in all the regions: surface, middle and interface, and the smallest amount of Cr and Mn. This result is in agreement with a previous study [22] on the oxidation kinetics of these samples, where the Mo-implanted sample exhibited the worst oxidation resistance. This is probably due to the formation of volatile molybdenum oxides, such as MoO_2 and MoO_3, at high temperatures, leading to

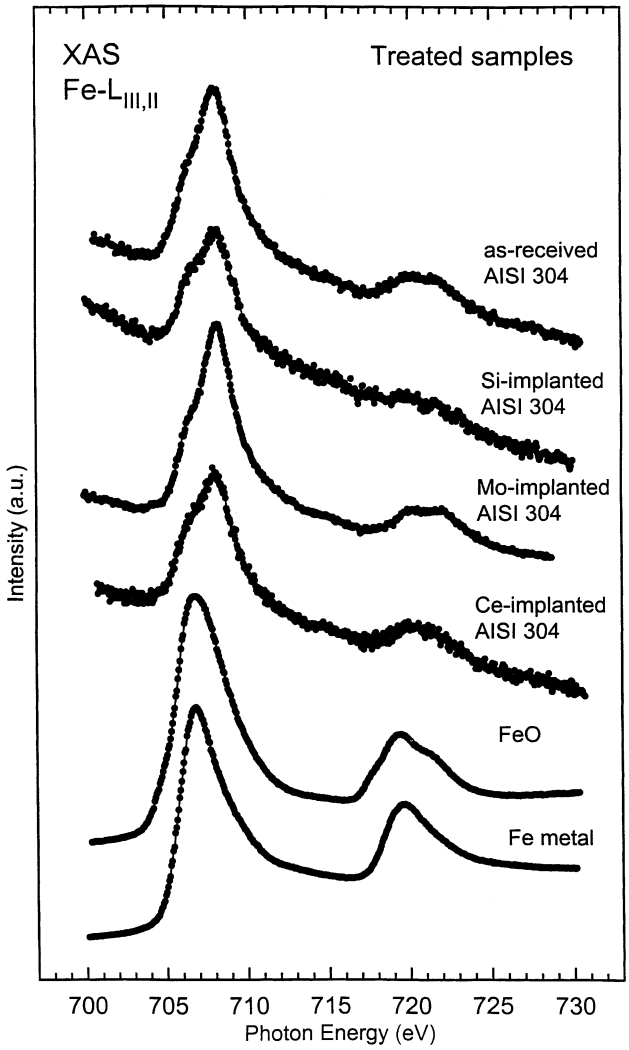

Fig. 4. Fe 2p soft X-ray absorption spectra of all heat-treated AISI 304 stainless steel samples: as-received and after Si, Mo and Ce ion implantation, and FeO and Fe metal samples for comparison.

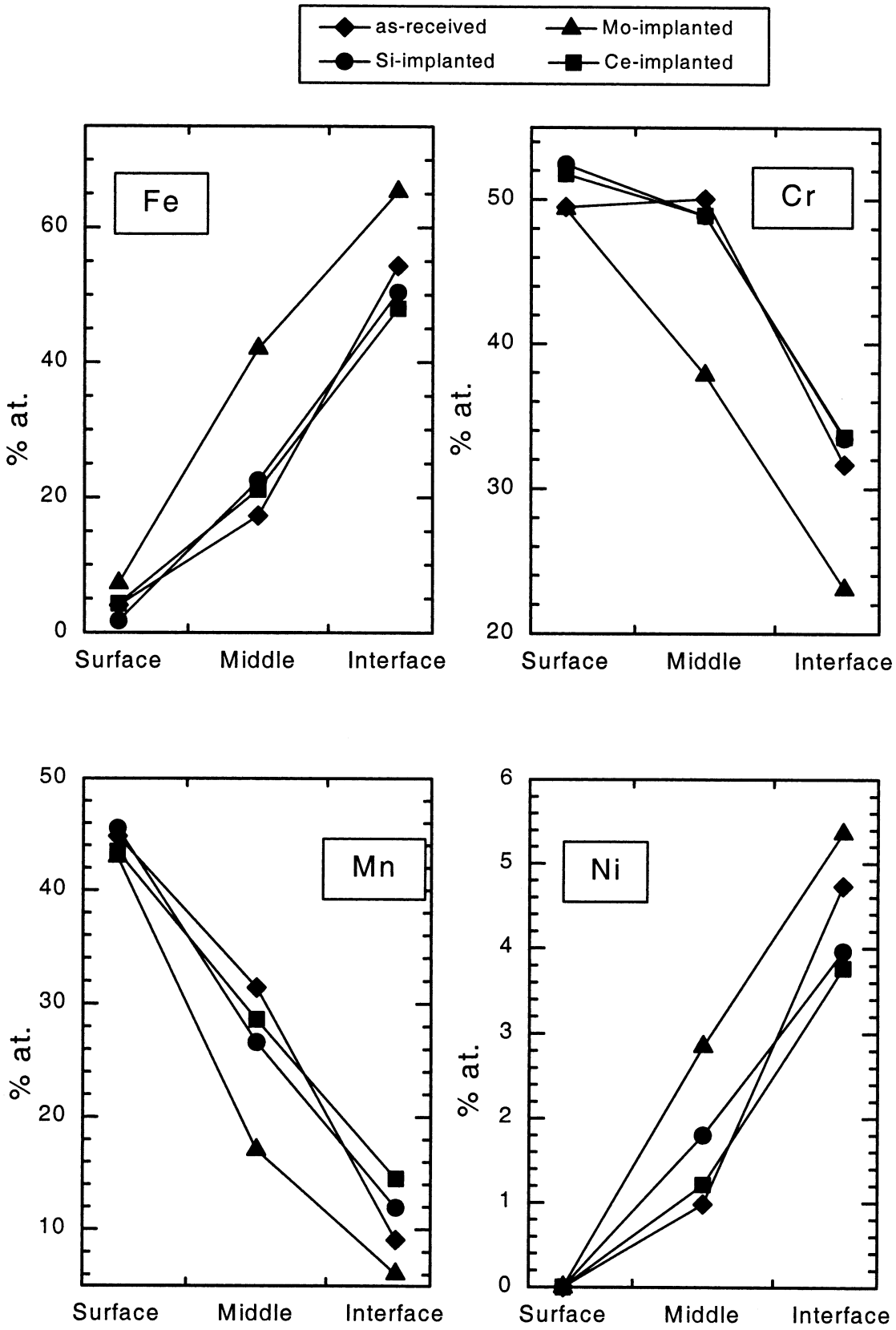

Fig. 5. Element composition percentage corresponding to Fe, Cr, Mn and Ni, for the heat-treated AISI 304 stainless steel, as-received and after Si, Mo and Ce ion implantation. Surface, middle and interface correspond to different regions in the oxide layer (see text).

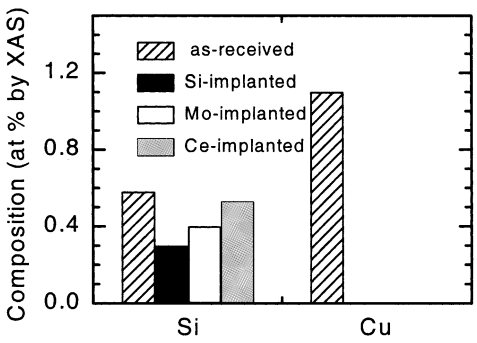

Fig. 6. Element composition percentage corresponding to Si and Cu, for the heat-treated AISI 304 stainless steel, as-received and after Si, Mo and Ce ion implantation.

catastrophic oxidation of the material [18]. In this case the oxide layer obtained after the thermal treatment is less homogeneous than in the other samples. Finally, the presence of Ni is mainly observed in the interface region, gradually decreasing until its signal disappears at the surface region. This result suggests that no Ni diffusion from the metal to the surface during oxidation takes place.

Fig. 6 shows the values of the percentage composition corresponding to the Si and Cu XAS signals that were found in minor proportions. Both signals were obtained in an appreciable quantity only in the surface of the oxide scale. In Figs. 5 and 6 the percentage values of Ce and Mo do not appear, because their XAS signals were negligible. However, as the average depth of the implanted elements is larger than the XAS probing depth, no XAS emission for these implanted elements was expected. This result also indicates that, during oxidation, diffusion of implanted Ce and Mo from the metal to the oxide–metal interface or to the oxide layer does not occur. Assuming that Ce and Mo remain at the metal–oxide interface, the diffusing species (C^{3+}, Fe^{2+}, Fe^{3+}, Ni^{2+} and Mo^{2+}) migrate according to their relative concentration in the oxide, at a rate determined by the chemical potential and the value of the diffusion coefficient, showing a possible transition from internal to external oxidation [23]. The case of the Si signal is, however, different, because Si is a constituent of AISI 304 stainless steel and because of a higher implantation dose.

Fig. 6 shows an appreciable Cu content only in the case of the non-implanted sample. This result suggests Cu diffusion from the metal to the oxide layer during the oxidation process, which takes place only for the non-implanted sample. However, this Cu diffusion is less evident in the case of the implanted samples, suggesting the formation of a barrier by the ion implantation process. Moreover, implanted samples probably resulted in different oxide-layer thickness for equivalent exposure, due to different implant profiles and surface damage on the material surface.

4. Conclusions

- TRIM calculations have shown that the final distribution of each implanted ion on the AISI 304 steel substrate depends on the specific ion. Such final implanted distribution may account for the subsequent oxidation behaviour, i.e. the lowest penetration of Ce ions promotes the formation of a more protective oxide layer in comparison with that of Si. However, the presence of Mo induces a negative effect, probably due to the volatilisation of molybdenum oxides.
- By comparing the oxidised specimens, EDS analysis has also shown that Si and Ce ion implantation induces Cr and Mn enrichment. Transformation from the austenite matrix phase into a ferrite phase is probably due to Cr as a ferrite stabiliser. Mo implantation, however, promotes the formation of Fe-enriched oxides, leading to poorer oxidation behaviour. SEM showed compact oxide layers in all specimens, except in the case of Mo implantation. It seems that volatilisation of the molybdenum oxides may again account for this.
- The XAS spectra show Cr and Mn as main constituents of the outermost oxidised layer. This result is in agreement with conventional XRD, where the presence of Cr–Mn spinel oxides was observed.
- The poor Fe XAS signal in the outermost region of the oxidised layer indicates less favoured Fe diffusion compared to that of Cr or Mn, probably due to variation in the chemical potential of oxygen through the oxide layer.
- An appreciable Cu signal was detected by XAS in the non-implanted and oxidised steel, which was not present in any of the implanted and oxidised specimens. This result suggests that the implantation process itself modifies the diffusion mechanisms upon high-temperature oxidation.

References

[1] F.G. Geib, R.A. Rapp, Oxid. Met. 40 (1993) 213.
[2] D.P. Whittle, J. Stringer, Phil. Trans. R. Soc. Lond. A 295 (1980) 309.
[3] P.A. Choquet, M.A. Harper, R.A. Rapp, J. Phys. 50 (1989) 681.
[4] R.G.I. Leferink, W.M.M. Huijbregts, Corros. Sci. 35 (1993) 1235.
[5] J. Stringer, Mater. Sci. Eng. 87 (1987) 1.
[6] J. Stringer, Surface Engineering, Series E, Applied Science No 85, Martinus Nijhoff Publishers, Dordrecht, 1984.
[7] J.M. Hampikian, D.I. Potter, Oxid. Met. 38 (1992) 125.
[8] T.A. Crabb, P.N. Gibson, E. MacAlpine, Corros. Sci. 35 (1993) 1541.
[9] X. De Buchere, P. Andreazza, C. Andreazza-Vignole, C. Clinard, R. Erre, Surf. Coat. Technol. 80 (1996) 49.

[10] S. Seal, S.K. Bose, S.K. Roy, Oxid. Met. 41 (1994) 139.
[11] Y. Saito, B. Önay, T. Maruyama, J. Phys. IV 3 (1993) 217.
[12] M. Abbate, J.B. Goedkoop, F.M.F. De Groot, M. Grioni, J.C. Fuggle, S. Hofmann, H. Petersen, M. Sacchi, Surf. Interface Anal. 18 (1992) 65.
[13] S.L.M. Schroeder, Solid-State Commun. 98 (1996) 405.
[14] J.C. Fuggle, J.E. Inglesfield, Unoccupied Electronic States, Springer, Berlin, 1991.
[15] M. Abbate, F.M.F. De Groot, J.C. Fuggle, A. Fujimori, Y. Tokura, Y. Fujishima, O. Strebel, M. Domke, G. Kaindl, J. van Elp, B.T. Thole, G.A. Sawatzky, M. Sacchi, N. Tsuda, Phys. Rev. B 44 (1991) 5419.
[16] Z.Y. Wu, S. Gota, F. Jollet, M. Pollak, M. Gautier-Soyer, C.R. Natoli, Phys. Rev. B 55 (1997) 2570.
[17] Kirk-Ohmer Encyclopaedia of Chemical Technology, 4th ed., John Wiley & Sons, New York, 1995, p. 783.
[18] H.J. Grabke, G.H. Meier, Oxid. Met. 8 (1995) 147.
[19] F.J. Pérez, M.J. Cristóbal, M.P. Hierro, F. Pedraza, G. Arnau, P. Merino, Surf. Coat. Technol. 126 (2000) 116.
[20] L. Soriano, M. Abbate, F.M.F. De Groot, D. Alders, J.C. Fuggle, S. Hofmann, H. Petersen, W. Braun, Surf. Interface Anal. 20 (1993) 21.
[21] A.D. Pelton, H. Schmalzriel, J. Sticher, J. Phys. Chem. Solids 40 (1979) 1103.
[22] A. Gutiérrez, M.F. López, F.J. Pérez Trujillo, M.P. Hierro, F. Pedraza, Surf. Interface Anal. 30 (2000) 130.
[23] N. Birks, G.H. Meier, Introduction to High-Temperature Oxidation of Metals, E. Arnold, 1982.